

# HIGH ENERGY SOLAR PARTICLE EVENTS AND THEIR ASSOCIATED CORONAL MASS EJECTIONS

P.K. MANOHARAN and G. AGALYA

*Radio Astronomy Centre, National Centre for Radio Astrophysics,  
Tata Institute of Fundamental Research, Udhamandalam (Ooty), India.*

Intense solar energetic particle (SEP) events data, associated with ground level enhancements (GLEs), occurred during 1989 to 2006 have been obtained from the spectrometers on board GOES spacecraft in the energy range 10–100 MeV. The interplanetary effects of these events and their associated coronal mass ejections (CMEs) have been provided by the LASCO/SOHO coronagraph images in the field of view of 2–30  $R_{\odot}$  and the interplanetary scintillation images from the Ooty Radio Telescope in the heliocentric distance range of  $\sim 40$ –250  $R_{\odot}$ . The comparison between the radial evolution of the CME and its associated particle spectrum shows that the spectrum is soft at the onset of the particle event. A flat spectrum is observed at the peak of the particle event and the spectrum becomes steeper as the CME moves farther out into the inner heliosphere. However, the magnitude of change in spectral slopes differs from one CME to the other, suggesting the difference in energy available within the CME to drive the shock. The spectral index evolution as a function of initial speed of the CME at different parts of the particle profile has also been compared. The result shows that the change in particle flux with time is rather quick for the high-energy portion of the spectrum than that of the low-energy part, which makes the steepening of the energy spectrum with time/distance from the Sun. It indicates that the acceleration of particles by a CME-driven shock may be efficient at low energies ( $\leq 30$  MeV) and the efficiency of the shock decreases gradually towards the high-energy side of the spectrum.

*Keywords:* solar flares, coronal mass ejections (CMEs), CME speed evolution, solar energetic particles (SEPs), particle acceleration, particle energy spectrum

## 1. Ground Level Enhancements and SEP Events

The physical mechanisms involved in the production and acceleration of solar energetic particle (SEP) events are rather complex and not yet fully understood. In general, SEP events are associated with explosive phenomena taking place on the Sun, such as flares and coronal mass ejections (CMEs). There are two types of SEP events, impulsive and gradual events<sup>1</sup>. Impulsive events have their origin at the rapid and short-lived (duration  $\leq 30$

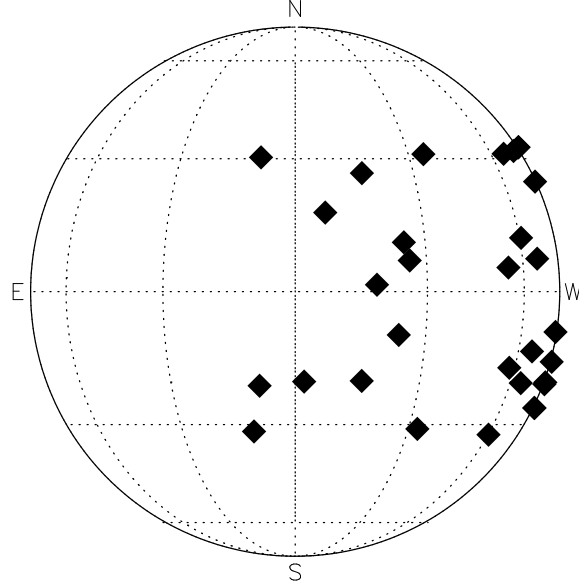


Fig. 1. Location of SEP events associated with GLEs observed between 1989 and 2006. The position of origin of all these events located to the western side of the Sun essentially suggests the magnetic connectivity between the source location of particle event and the observing point near the Earth.

min) flare events, which are dominated by electrons,  $^3\text{He}$ , and heavy ions. The energy release processes associated with the flare play a key role in the impulsive acceleration of particles. In the case of gradual events, they have association with CME/flare events, which are rich in protons, and the CME-driven shocks accelerate particles in the interplanetary space<sup>2</sup>. There are several excellent articles and reviews on solar particle events<sup>3-6</sup>.

A large and energetic flare/CME associated with an intense gradual SEP event is important because it can give rise to cosmic ray ground level enhancements (GLEs). For example, GLEs involve the hard spectrum of protons (at energies  $>1$  GeV) and can be detected by neutron monitor on the Earth. In this study, we concentrate on the evolution of intense particle events in the Sun-Earth distance. For example, the GLE can be used as an indicator of the associated intense particle event. We have selected 31 SEP events associated with GLEs in the period 1989 to 2006. The GLE has been only used as an indicator for intense particle event. The main focus is however on the comparison of temporal variation of energy spectrum of SEP events with the propagation properties of CMEs in the near-Sun

region as well as in the Sun-Earth interplanetary space.

## 2. Event Selection and Analysis

In this study, we consider 31 SEP events associated with ground level enhancements (GLEs) occurred between 1989 and 2006. This period covers the second half of solar cycle 22 and the full extend of cycle 23. The solar proton measurements in the energy range of 10–100 MeV have been obtained from Geostationary Operational Environmental (GOES) spacecraft. The near-Sun images of CMEs associated with these SEP events, observed after the year 1997, have been obtained from the LASCO/SOHO C2 and C3 coronagraphs<sup>7</sup>, which cover the field of view of 2–30  $R_{\odot}$  (1 solar radius,  $R_{\odot} = 6.96 \times 10^5$  km). Whenever available, the interplanetary scintillation measurements at Ooty on a grid of large number of radio sources provide images of CME associated disturbances in the interplanetary space at different heliocentric distances until the arrival of the CME at the orbit of the Earth (i.e., up to  $\sim 250 R_{\odot}$ )<sup>8</sup>. The scintillation images in particular are extremely useful in understanding the radial evolution of CME in the inner heliosphere.

Table 1 shows the list of 31 SEP events under consideration. It includes conventional GLE number (<http://neutronm.bartol.udel.edu/>), classification of associated flare event, its location on the Sun, start of X-ray flux, CME onset time at the LASCO C2 coronagraph, type of the CME (full halo or partial halo), speed of the CME in the LASCO field of view, shock arrival at 1 AU, and start of the particle event as recorded by GOES spectrometer. As shown in the table, most of them have association with intense flares (except 3 events occurred at longitude  $>90^{\circ}$  west and they can not be accurately classified) and wide CMEs (width  $>180^{\circ}$ ). Figure 1 displays the flare location of events listed in Table 1. The remarkable crowding of SEP events to the western hemisphere of the Sun (at  $>10^{\circ}$  east longitude) is consistent with the magnetic connectivity between the particle acceleration site and the Earth, i.e., along the Archimedian spiral<sup>9</sup>.

## 3. Particle Data and CME Speed

Figure 2 shows an example of gradual SEP event, observed in association with a fast halo CME and an intense flare (X3.4/4B) that occurred on December 13, 2006 at S05W23 on the Sun. The X-ray onset of the flare at 02:14 UT on December 13 and the 1-AU arrival time of the CME-associated shock at 13:57 UT on December 14 are indicated by respective vertical lines on

Table 1. List of 31 SEP Events

		Date	Flare Data		CME Data			Shock at 1 AU		Particle Event	
No.	GLE No.		Class	Location	Start hh:mm	C2 Onset hh:mm	H/PH*	Speed kms <sup>-1</sup>	Date	Time hh:mm	Start Time hh:mm
1	40	25Jul89	X2.6/2N	N25W84	08:39				26Jul(?)	13:00(?)	09:00
2	41	16Aug89	X20/2N	S15W86?	01:08				17Aug	15:41	
3	42	29Sep89	X9.8/1B	S26W90	10:47				30Sep	17:16	12:05
4	43	19Oct89	X13/4B	S27E10	12:29				20Oct	09:16	13:05
5	44	22Oct89	X2.9/2B	S27W31	17:08						
6	45	24Oct89	X5.7/3B	S30W57	17:36				26Oct	14:27	
7	46	15Nov89	X3.2/3B	N11W26	06:38				17Nov	09:25	07:35
8	47	21May90	X5.5/2B	N35W36	22:12				25May	05:10	23:55
9	48	24May90	X9.3/1B	N33W78	20:46				26May	20:37	21:25
10	49	26May90	X1.4	W104?	20:45						
11	50	28May90	C 1.4	W130?	04:28				30May	09:04	07:15
12	51	11Jun91	X12/3B	N31W17	02:09				12Jun	10:12	
13	52	15Jun91	X12/3B	N33W69	06:33				17Jun	10:19	
14	53	25Jun92	X3.9/2B	N09W67	19:47				27Jun	20:35	20:45
15	54	02Nov92	X9		02:31				04Nov	13:12	
16	55	06Nov97	X9.4/2B	S18W63	11:49	12:10	H	1556	09Nov	10:00	13:05
17	56	02May98	X1.1/3B	S15W15	13:31	14:06	H	938	04May	02:03	14:20
18	57	06May98	X2.7/1N	S11W65	07:58	08:29	PH	1099	08May	09:20	08:45
19	58	24Aug98	X1/3B	N35E09	21:50				26Aug	06:36	23:55
20	59	14Jul00	X5.7/3B	N22W07	10:03	10:54	H	1674	15Jul	14:35	10:45
21	60	15Apr01	X14.4/2B	S20W85	13:19	14:06	PH	1199	18Apr	00:51	14:10
22	61	18Apr01	C2.2	S20WL	02:11	02:30	H	2465	21Apr	15:30	03:15
23	62	04Nov01	X1/3B	N06W18	16:03	16:35	H	1810	06Nov	01:45	17:05
24	63	26Dec01	M7/1B	N08W54	04:32	05:30	PH	1446	29Dec	06:20	06:05
25	64	24Aug02	X3/1F	S08W81	00:49	01:27	H	1913	26Aug	11:40	01:40
26	65	28Oct03	X17.2/4B	S16E08	09:51	11:30	H	2459	29Oct	05:58	
27	66	29Oct03	X10/ 2B	S15W02	20:37	20:54	H	2029	30Oct	16:20	
28	67	02Nov03	X8.3/2B	S14W56	17:03	17:30	H	2598	04Nov	05:53	
29	68	17Jan05	X3.8	N15W25	06:59	09:54	H	2547			
30	69	20Jan05	X7.1/2B	N14W61	06:36	06:54	H	2400	21Jan	16:48	
31	70	13Dec06	X3.4/4B	S05W23	02:14	02:54	H	1774	14Dec	13:57	03:10

Note: \* H - Halo CME; PH - partial halo CME.

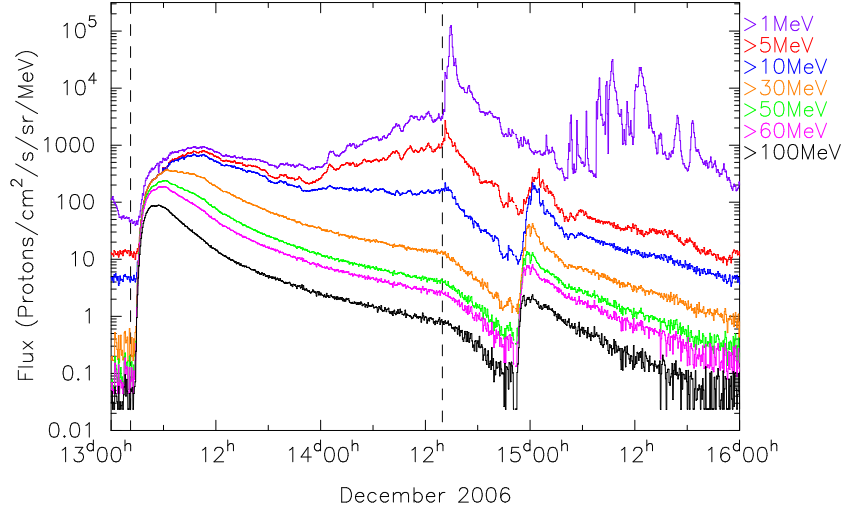


Fig. 2. GOES-11 proton flux measurements between 13 and 16 December 2006. The vertical line at 02:14 UT on December 13 indicates the time of X-ray onset of the flare event. Another vertical line identifies the arrival of interplanetary shock at 1 AU on December 14, 2006, at 13:57 UT. The particle energy increases from top to bottom curves (refer to right-hand side legend).

the plot. The low-energy protons ( $E < 10$  MeV) show gradual increase after about 0 UT on December 14, suggesting an increase in the efficiency of the shock-driven acceleration. Additionally, on the arrival of the interplanetary shock at the near-Earth space, low-energy protons show a sharp increase in flux, which is due to the increase in the population of energetic storm particles. However, after the passage of the shock all the energy channels show systematic decrease in proton flux.

In association with this intense flare event, LASCO/SOHO C2 coronagraph recorded the onset of a full halo CME at 02:54 UT on December 13. The second order polynomial fit to the height-time plot obtained from C2 and C3 images indicates a decrease in the sky-plane speed from 2000 to 1700  $\text{kms}^{-1}$  in the distance range of 2–20  $R_{\odot}$ <sup>10</sup>.

#### 4. SEP Energy Spectrum

As shown in Table 1, each SEP event was accompanied by a fast and wide CME. At the leading edge of the CME, a shock wave was observed and part of it passed through the Earth-orbiting satellite as an interplanetary shock. The arrival time of the shock at 1 AU is included in Table 1. For each event, based on the GOES spectrometer data, we have computed the energy spec-

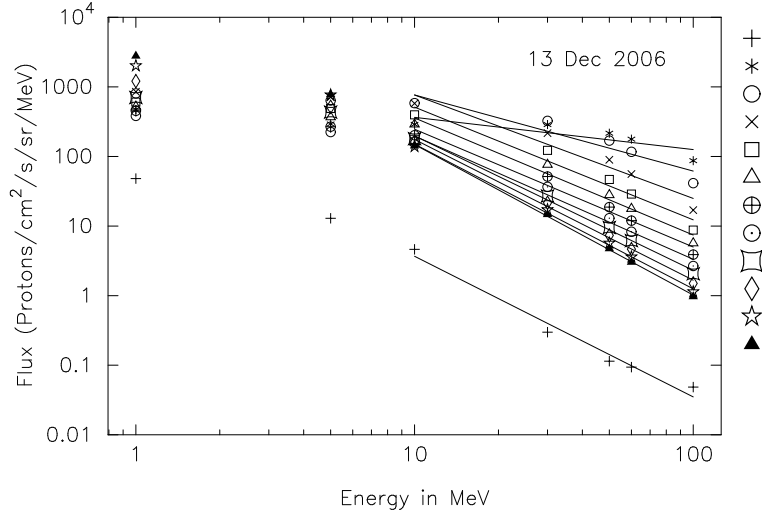


Fig. 3. The energy spectrum of the SEP event associated with the flare event on December 13, 2006. Each line in the plot is the least square fit to the proton measurements between 10 and 100 MeV. The symbols displayed at the right-hand side of the plot, from top to bottom respectively, represent 3-hour interval fits from the flare onset time to shock arrival at the Earth. It is evident that the overall particle flux decreases in all energy bands also the spectrum steepens as the CME moves away from the Sun.

trum of protons ( $E^\gamma$ ), in the energy range 10–100 MeV, nearly from the onset time of the particle event to the shock arrival time at the near-Earth space, approximately at every 3-hour interval. We need to consider the dispersion effects on the arrival time of particles from the acceleration site (i.e., at the shock front) to 1 AU. The travel time of the particle depends on its propagation path, the pitch angle and speed. For a typical background solar wind speed of  $\sim 400 \text{ km s}^{-1}$ , the spiral length corresponds to  $\sim 1.2 \text{ AU}$  in the Sun-Earth distance. It is known that high-energy particles ( $>10 \text{ MeV}$ ) experience relatively less pitch angle scatter than low-energy particles along the interplanetary magnetic field and therefore propagate more directly to 1 AU<sup>11</sup>. For all the events (except January 17, 2005), we have considered the spectral shape at each 3-hour interval on or after the peak of the particle profile. For the event on January 17, 2005, the peak of the particle profile is observed after  $\sim 9$  hours of the flare onset.

In order to study the spectral changes at every 3-hour interval over an energy range of 10–100 MeV, a least-square fit has been made to the  $\log(\text{flux})$ - $\log(\text{energy})$  plot to get the power-law form of the spectrum ( $\sim E^\gamma$ ). However, for some of the intervals, a simple power-law (i.e., single straight-

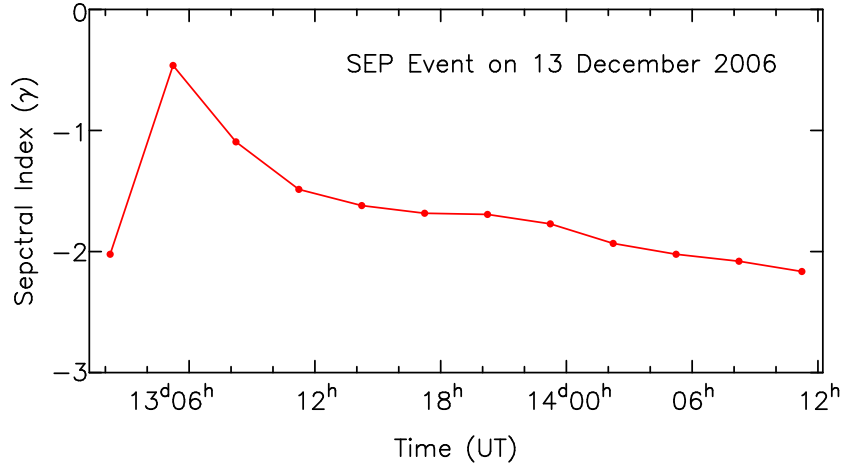


Fig. 4. Spectral index as a function of time for the SEP event on December 13, 2006. The spectral index has been obtained in the energy range 10–100 MeV. The spectrum is flat ( $\gamma = -0.5$ ) at the peak of the particle profile and spectrum steepens with time or as the CME propagates away from the Sun.

line fit) was not adequate. Since the primary aim is to study the change in the overall spectral shape as a function of time, an average power-law fit has been made to the spectrum in the range 10–100 MeV. Figure 3 shows the spectral fittings in the energy range of 10 to 100 MeV at consecutive 3-hour intervals for the SEP event observed on December 13 and 14, 2006. At the initial phase of the SEP event, i.e., just after the particle onset, the spectrum looks soft and the particle flux at high-energy portion increases with time.

#### 4.1. Radial Evolution of SEP Spectrum

In Figure 4, spectral indexes observed at consecutive 3-hour intervals are plotted for the SEP event associated with the flare event on December 13, 2006. This plot includes spectral index nearly from the particle onset time to the shock arrival at the Earth. The spectrum attains the maximum flatness at the peak of the particle profile, spectral index,  $\gamma \approx -0.5$ , and the spectral index decreases as the CME propagates away from the Sun.

Another interesting point is that the particle flux at all energy bands decreases with time. It is likely linked to the shock ahead of the CME event. As the CME propagates, the shock strength (as well as the compression ratio in the sheath region) decreases with time/heliocentric distance. However, the difference in reduction of particle at the low-energy side of

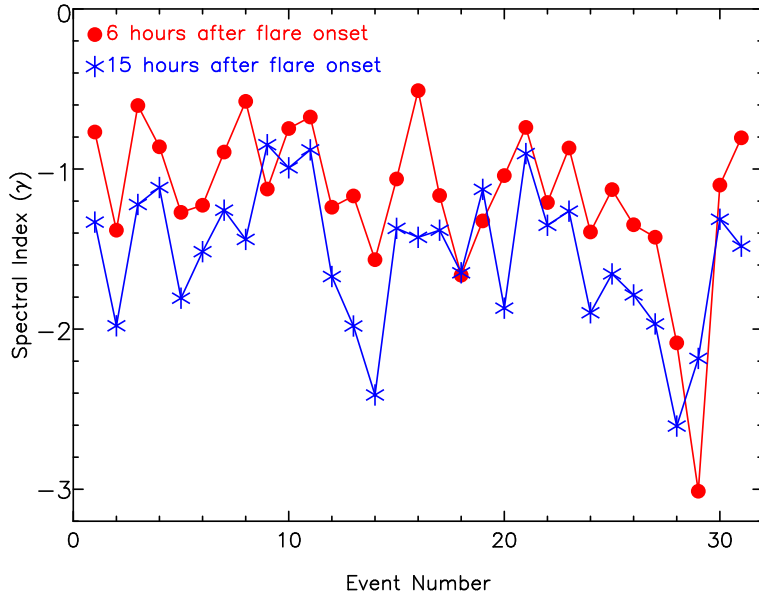


Fig. 5. Spectral index as a function of event number. The x-axis gives the event numbers as listed in Table 1. The filled-circle and star symbol represent, respectively, the spectral indexes at 6 and 15 hours after the flare onset. It is evident from these plots that most of the spectra (28 out of 31 events) are steeper at large distance from the Sun.

the energy spectrum (i.e.,  $\sim 10$  MeV) is less between the peak of the profile and the shock arrival time (i.e., typically about an order of magnitude reduction is observed). Whereas at the high-energy portion of the spectrum (i.e.,  $\sim 100$  MeV), the decrease in particle flux is more than or  $\sim 2$  orders of magnitude. This suggests that only soft protons are produced at the front of the CME-driven shock as the CME propagates to large distance. The systematic changes in the particle flux and spectral index suggest a decrease in the efficiency of acceleration by the shock driven at the front of the CME. The above observed trend is compared with the speed evolution of the CME in the Sun-Earth distance.

## 5. Spectral Evolution with Time/Heliocentric Distance

Figure 5 shows the plots of spectral indexes of 31 SEP events at 6 and 15 hours after the flare onset time. It is evident that out of 31 SEP events, 28 of them show steepening of the energy spectrum with time as the CME propagates to larger distance from the Sun. However, the relative steepening differs from one CME to the other, suggesting that the CME-driven shock



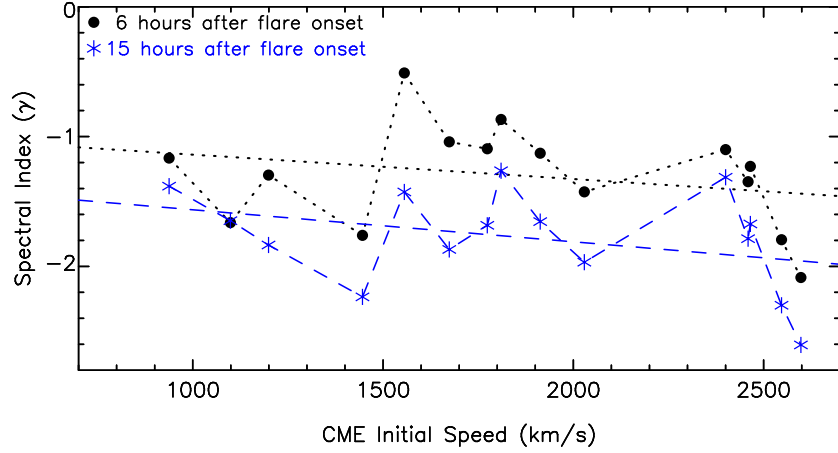


Fig. 6. Spectral indexes at 6 hour and 15 hour after the flare event are plotted against initial speed of the CME. The initial speeds have been obtained from LASCO C2 and C3 white-light images and cover a range of 900 to 2600  $\text{km s}^{-1}$ . As shown in Figure 5, the energy spectrum is flat at near the Sun (6 hours after the flare onset) and becomes steep as the CME propagates to large distance (15 hours after the flare onset). The least square straight line fits to 6-hour and 15-hour indexes are shown, respectively, by dotted and dashed lines.

or energy available for the acceleration of particle is CME dependent, which can be mostly related to the magnetic energy possessed by the CME as well as the expansion rate of the CME.

The other 3 cases showing flattening at large distances are on 24 May 1990 (event #9), 24 August 1998 (event #19), and 17 January 2005 (event #29). As it is clear from Figure 5, events #9 and #19 go through only a marginal flattening, where as the event #29 on January 17, 2005, shows heavy flattening with distance from the Sun. It is to be noted that in this SEP event, the particle flux peaked at about 9 hours after the flare peak. Therefore the spectral index measured at 6 hours after the flare event is associated with the growth phase of the particle profile. It is also be noted that the CME on January 17, 2005, shows likely interaction with a preceding CME, which originated nearly from the same location. It is inferred that the particle profile of this event has been heavily influenced by the effects of interaction<sup>12</sup>.

## 6. CME Speed and Spectral Index Changes

In this study, we have considered CMEs observed between 1989 and 2006. However, the speed measurements are available for CME events observed

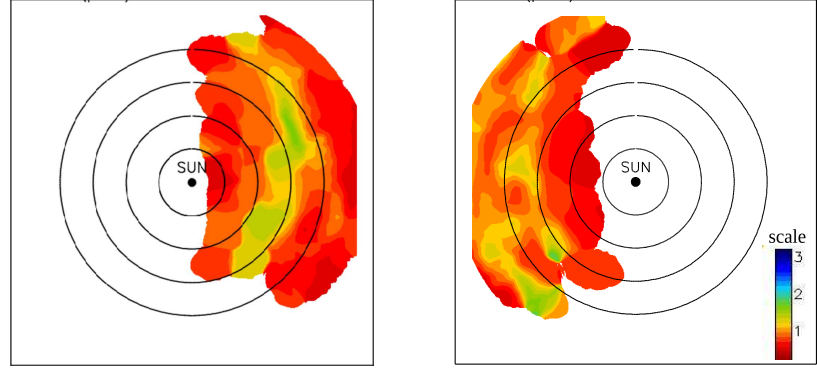


Fig. 7. IPS images of disturbance associated with the CME event on December 13, 2006 and they correspond to IPS measurements at  $\sim 0$  UT (left image) and  $\sim 14:30$  UT (right image) on December 14, 2006. In these ‘Position Angle – Heliocentric Distance’ plots, the Sun is at the center. The concentric circles are 50, 100, 150, and 200  $R_{\odot}$ . At the LASCO C2 field of view, the CME onset was observed at 02:54 UT on December 13, 2006. As seen in the above images CME has expanded and moved to larger distances with time.

after the year 1997 (i.e., after the advent of LASCO/SOHO mission). The LASCO C2 and C3 white-light images provide the initial speed of the CME at distances  $\leq 30 R_{\odot}$ . In Figure 6, we plot the spectral index as a function of initial speed of the CME. The spectral indexes after 6 hours of the flare event are shown by filled-circle symbols and star symbols represent spectral shape after 15 hours of the flare onset. As indicated by Figure 5, the energy spectrum is steeper at the large distance from the Sun than that of its starting phase close to the Sun and the same trend is observed for the range of initial speeds between 900 and 2600  $\text{kms}^{-1}$ . The straight lines shown in the plot are least square fits to the indexes at 6-hour (dotted line) and 15-hour (dashed line), respectively. These fits show marginal steepening with speed. However, at speeds above 2500  $\text{kms}^{-1}$ , two events show steeper spectra, which require more investigations.

### 6.1. Interplanetary Scintillation Images

The interplanetary scintillation (IPS) measurements on a large number of radio sources are useful to image disturbances associated with a propagating CME in the distance range of  $\sim 40$ – $250 R_{\odot}$ <sup>8,13</sup>. Figure 7 shows sample images of the inner heliosphere associated with the CME event on December 13, 2006. These are ‘position angle – heliocentric distance’ images and the Sun is at the center. The concentric circles are, respectively, 50, 100, 150,

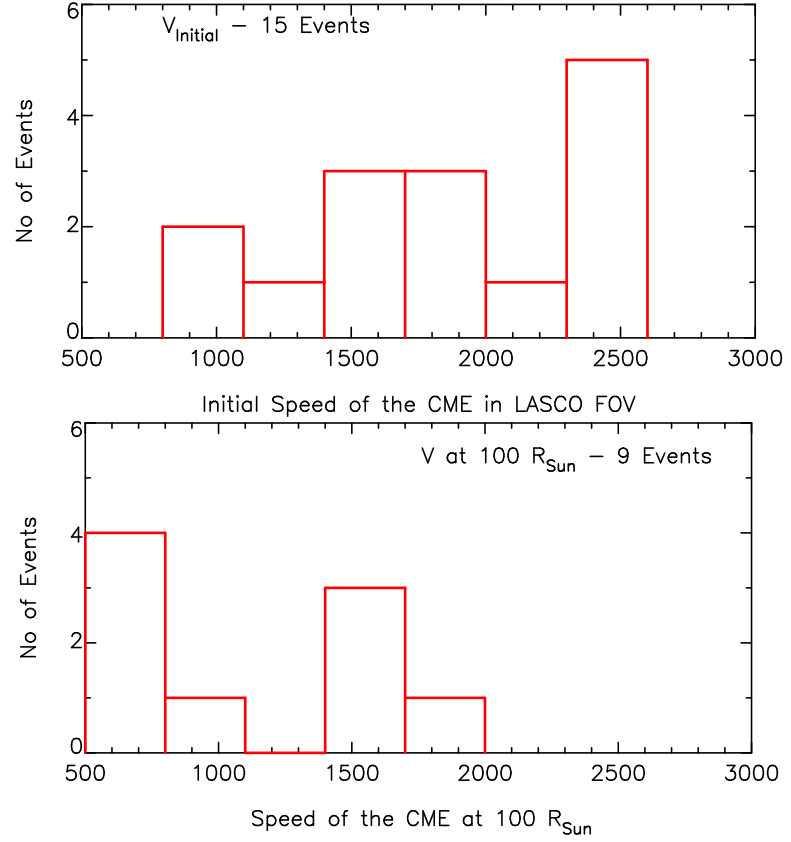


Fig. 8. Histograms of initial speed of the CME in the LASCO field of view and speed at  $\sim 100 R_{\odot}$ . The initial speeds are high  $\geq 900 \text{ km s}^{-1}$  and cover a wide range  $\sim 900\text{--}2600 \text{ km s}^{-1}$ . At distance  $\sim 100 R_{\odot}$ , the propagation speed tends to reduce, indicating the energy exchange between the CME and solar wind and/or the drag force experienced by the CME in the ambient solar wind.

and  $200 R_{\odot}$ . These images are made from the normalised scintillation index (denoted by  $g$ ) measurements obtained from a grid of large number of radio sources ( $\sim 1000$  sources per day)<sup>8</sup>. The increase in the value of normalised scintillation index indicates the presence of CME associated disturbance. The color-code scale shown in Figure 7 from red to blue represents the background solar wind ( $g \approx 1$ ) to an increased level of density and/or density turbulence ( $g \approx 3$ ). The image at the left of the figure corresponds to IPS measurements on December 14, centered around 0 UT and the right image represents the position of CME associated disturbance  $\sim 14:30$  UT

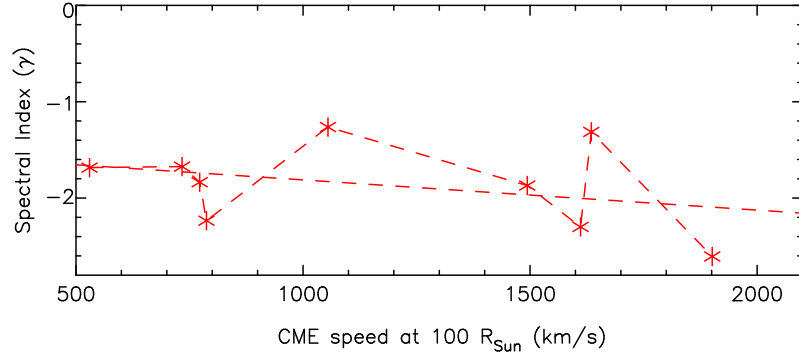


Fig. 9. Spectral index measured at 15 hours after the flare event is compared with the IPS speed of the CME at  $\sim 100 R_{\odot}$ .

on the same day. In each image, the time increases from the right-hand side of the image (west of the Sun) to the left-hand side of the image (east of the Sun). For example, the snapshot of a halo CME at a given time will appear as a ring around the Sun<sup>8</sup>. A halo CME observed at the west expands to larger distance with time. The difference in distance seen between 0 UT and 14:30 UT images shows the propagation of the CME. The halo CME expansion/propagation to farther distance with time is evident in these images.

As in the case of LASCO images, the above such IPS images can also be used to obtain the onset time of CME at different distances from the Sun and the ‘*heliocentric distance – time*’ plot can provide the speed profile of the CME in the inner heliosphere<sup>8</sup>. In the present study, we compare the properties of the particle events at the near-Sun region (based on LASCO field of view speed) and at  $\sim 100 R_{\odot}$  (based on IPS estimates). For some selective events, which have both LASCO and IPS measurements, the histograms of initial speed and speed at  $\sim 100 R_{\odot}$  are plotted in Figure 8. The initial-speed plot covers a range 900–2600  $\text{kms}^{-1}$ . However, as the CME propagates to  $\sim 100 R_{\odot}$ , the speed tends to reduce. As shown by Manoharan<sup>8</sup>, the drag force experienced by the CME due to the interaction with ambient solar wind essentially slows the CME. In other words, the energy exchange between the CME and solar wind plays a major role in shaping the speed profile of the CME with time/distance from the Sun. Moreover, it is likely that the energy exchange between the CME and the ambient solar wind can be quick for an extremely high-speed event<sup>8</sup>.

In Figure 9, the spectral index observed at 15 hours after the solar event has been compared with speed obtained from IPS at  $\sim 100 R_{\odot}$ . Although

this plot includes only 9 events, it shows similar trend seen in the near-Sun region (refer to Figure 6). The range of speeds at this distance tends to narrow to the lower side and the energy spectrum is steeper than that of the near-Sun spectrum.

## 7. Summary and Conclusion

In this study, we have selected 31 intense SEP events associated with GLEs occurred during 1989 – 2006. All these gradual particle events had association with intense flares/CMEs, which originated towards the western side of the Sun (at longitude  $>10^\circ$  east), confirming the importance of the magnetic connectivity between the particle acceleration source region and the observing point at the Earth. These CMEs are fast and wide (halos and partial halos having width  $>180^\circ$ ). Their speeds cover the range between 900 and 2600  $\text{kms}^{-1}$ . The associated flares are also intense, most of them having X classification. The results show that the energy spectrum in the range 10–100 MeV is flat near the peak of the particle flux profile and as the CME propagated outward from the Sun, the spectrum steepens.

As the CME propagates, the high-energy particle flux decreases quickly than the low-energy particle flux, which shows that at the shock front the acceleration of low-energy particles is efficient. The rate of steepening of the spectrum varies from one event to the other, suggesting the energy available with each event is determined by the internal energy and the CME-driven shock to accelerate the particle.

The spectral index compared with the initial speed of the CME in the LASCO field of view shows rather marginal steepening with speed. The similar trend is observed at 6 and 15 hours after the flare onset. Also in the IPS field of view, at  $\sim 100 R_\odot$ , the spectrum is steeper than the 6-hour spectrum. Further the speed distribution of CMEs at the LASCO field of view ( $R \leq 30 R_\odot$ ) in the range 900–2600  $\text{kms}^{-1}$  tends to narrow to  $<2000 \text{ kms}^{-1}$  at  $\sim 100 R_\odot$ . Most of the events attain speeds below 750  $\text{kms}^{-1}$ . It essentially shows the effect of drag force applied by the ambient or background solar wind in slowing down the CME-driven shock. However further investigations are required to understand the dependence of particle spectrum on the initial speed of the CME.

## Acknowledgments

The authors acknowledge the observing/engineering staff of the Radio Astronomy Centre for help in making the IPS observations. We are grateful

to the GOES team for making the particle data available on the website. SOHO is a project of international cooperation between ESA and NASA. The authors would like to thank for the excellent LASCO-CME Catalog generated and maintained by the Center for Solar Physics and Space Weather, Catholic University of America, in cooperation with NASA and Naval Research Laboratory. This work is partially supported by the CAWSES-India Phase II Program, sponsored by the Indian Space Research Organisation (ISRO).

### References

1. Kallenrode, M.B., *J. Phys. G: Nucl. Part. Phys.* **29** (2003) 965-981.
2. Reames, D.V., et. al., *ApJ* **491** (1997) 414-420.
3. Reames, D.V., *Space Sci. Rev.* **90** (1999) 413-491.
4. Reames, D.V., *Sol. Phys.* **265** (2010) 187-195.
5. Miroshnichenko, L. I., Perez-Peraza, J. A., *International Journal of Modern Physics A* **23** No. 1 (2008) 1-141.
6. Shea, M. A., Smart, D. F., *Sol. Phys.* **127** (1990) 297-320.
7. Brueckner, G. E., et al., *Sol. Phys.* **162** (1995) 357-402.
8. Manoharan, P.K., *Sol. Phys.* **235** (2006) 345-368.
9. Reames, D.V., Barbier, L.M., Ng, C.K., *ApJ* **466** (1996) 473-486.
10. Manoharan, P.K., *Sol. Phys.* **265** (2010) 137-157.
11. Posner, A., Kunow, H., *Proc. 28th Intern. Cosmic Ray Conf.* **4** (2003) 3309-3312.
12. Gopalswamy, N., et. al., *ApJ* **572** (2002) L103-L107.
13. Manoharan, P.K., Tokumaru, M., Pick, M., et. al., *ApJ* **559** (2001) 1180-1189.